MARSWRF: A GENERAL PURPOSE, LOCAL TO GLOBAL NUMERICAL MODEL FOR THE MARTIAN CLIMATE AND ATMOSPHERE. A. Toigo[1], M. I. Richardson[2], and C. E. Newman[2], [1]Cornell University, Ithaca, NY 14853, (toigo@astro.cornell.edu), [1]Division of Geological and Planetary Sciences, California Institute of Technology, Pasadena, CA 91125 (mir@gps.caltech.edu, claire@gps.caltech.edu).

Introduction: A new planetary atmospheric numerical model, "MarsWRF," has been developed by modifying the National Center for Atmospheric Research (NCAR) Weather Research and Forecasting (WRF) model. The model has generalized map-projection, multi-scale, and nesting capabilities, blurring the distinction between global-, meso-, and micro-scale models, and enabling investigation of coupling between processes on all scales. The model can also be run in one, two or three dimensions.

The model has many advantages over previous models used by our research group [1,2], but differs significantly by virtue of its generalized map-projection, multi-scale and nesting ("zooming" in to higher resolution over part of the domain) capabilities, obviating the distinction between global and mesoscale models. As such, the model enables investigation of coupling between processes on a variety of scales, including global. The generalized computational grid also allows the model to be configured in one-, two-, or three-dimensional mode at runtime, allowing the impact of dimensionality and validity of modeled physical processes to be tested without the complication of switching model dynamical cores (e.g., Lagrangian vs. Eulerian) or numerical solvers (e.g., leap-frog vs. Runge-Kutta).

The Weather Research and Forecasting (WRF) Model: The original WRF model is a co-development of NCAR, the National Oceanographic and Atmospheric Administration (NOAA), the US Department of Defense, and various universities [3,4]. WRF is a state of the art mesoscale model used for both research and operational forecasting, this dual purpose being a key design feature intended to speed the application of new scientific and modeling developments into practical forecasting usage. The code is written primarily in Fortran 90, and has been designed to run on a variety of single processor, and distributed- and shared-memory parallel processor computers. The model, while being written completely from scratch, is intended to supersede the previous NCAR-managed Mesoscale Model Version 5 (MM5), and inherits much knowledge gained through more than 20 years' use of that model, including improvements in dynamical cores and physical parameterizations.

Although originally designed as a mesoscale model, the WRF dynamical core is quite general and appropriate for treatment of fluid flow on scales from meters to thousands of kilometers. The core integrates the fully-compressible, Euler equations in flux form. The full three-dimensional Coriolis and curvature effects are treated. WRF is a grid point model based around a horizontal Arakawa C-grid [5]. In the vertical, the terrain-following hydrostatic pressure ("eta") coordinate is used [6]. For horizontal calculations, 5th order advection is typical and time integration typically uses a 3rd order Runge-Kutta scheme, with a sub-timestep treatment of acoustic and fast gravity wave modes [3]

WRF has been designed to be flexible from the perspective of boundary condition definition and map projection. Run-time options to implement periodic, symmetric, open, and forced boundary conditions exist. WRF also includes the infrastructure necessary for the run-time definition of multiple parallel and downward levels of nesting, with one- or two-way interactivity and the option of nest motion within the mother domain.

Modifications of WRF for Global and Martian Application: While WRF has many of the required attributes for a truly comprehensive modeling system, it had two major drawbacks for our purposes: it was not configured such that a fully global domain could be simulated, and was written to be exclusively applicable to the Earth. Thus development work was done to make the model more general in use of map projections, implementing a new boundary condition at the poles of a global grid, generalization of model constants and timing conventions.

Non-conformal map projections. The simple cylindrical map projection that is used for most grid-point GCMs is a non-conformal projection, and indeed, any grid that seeks to represent the full globe on a single, rectangular domain must be non-conformal. Generalization of the model so that non-conformal map projections can be used required the equations to be rewritten with the full, separate x- and y-directional map scale factor components. Although implemented primarily to allow WRF to run with a traditional latitude-longitude (simple cylindrical) GCM map projection, the modifications allow any generalized map projection to be used.

Polar boundary conditions. Using a simple cylindrical map projection, a grid-point domain can be defined that uniformly covers the globe in latitude-longitude space. The eastern and western borders are actually same, and the boundary conditions there are periodic. On the northern and southern edges, a polar boundary condition was needed, and we have implemented one following the convention for C-grid models used, for example, by the GSFC Aries model [7]. In this mechanism, the northernmost C-grid staggering of the meridional velocity is the rotational pole, and the value of the meridional velocity at that point is constantly equal to zero. Since the grid distance at this point is zero, it should be noted that having a zero velocity at that point is zero does not preclude advection of material across the pole. Instead, advection through this region is accomplished by zonal transport within the most poleward zone.

Generalized planetary parameters and calendars. Obviously, constants relating to fundamental properties of the atmosphere (e.g., R, c_p, etc.) were changed throughout the

model. Beyond that, since the length of a day is different on Mars, some conversion for how dates and times are handled was necessary. For timekeeping, a day in the model is equivalent to one Martian sol, and the sol is broken up into 24 parts called "hours" for simplicity, and those hours broken up into 60 "minutes" for continued simplicity. The length of a second as used by all physical calculations remains unchanged. Additionally, for determining the solar insolation as it varies due to the planet's obliquity and orbital eccentricity, solar longitude (L_s) is calculated.

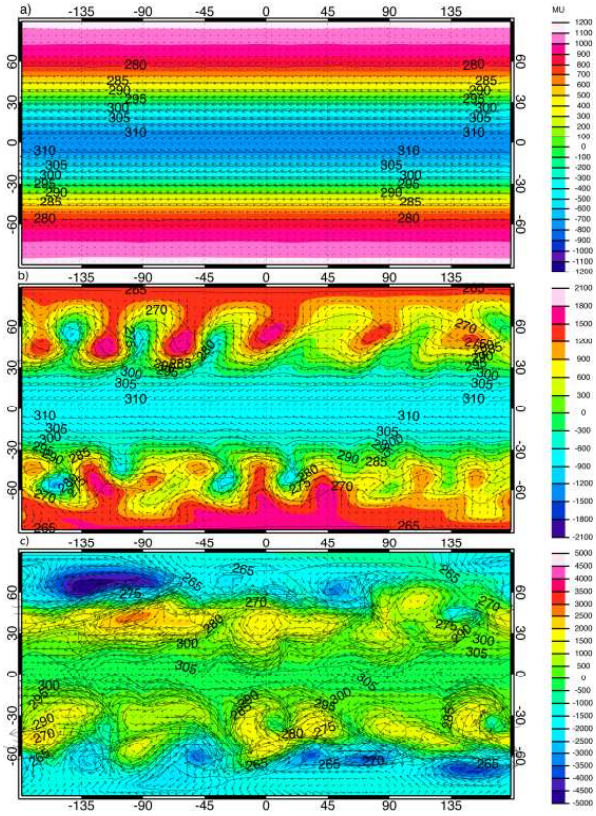

Figure 1: The WRF Held and Suarez [8] validation test simulation. In each subfigure the surface pressure perturbation, near-surface air temperatures, and near surface wind vectors are shown as background coloring, black contours and black arrows, respectively. a) The initially zonally symmetric fields (at 30 days after the start of the simulation), yield to b) the development of quasi-periodic instabilities in the mid latitude jets (60 days into the simulation), which c) ultimately settle into steady-state turbulence involving baroclinic frontal storm systems (shown here at 1 year into the simulation).

The "Held-Suarez" test of a dynamical core: The basic diagnosis of dynamical core behavior using the simplified prescribed forcing suggested by Held and Suarez [8] has become a standard test for new models. The test uses highly simplified parameterizations of atmospheric heating (Newtonian relaxation to a prescribed temperature profile) and boundary layer friction (Rayleigh damping of low level winds). The results consist of long-term averages (1000 days, following a 200 day spin up) of zonal-mean zonal winds and temperatures, and some eddy statistics.

The results from the WRF simulation of the Held and Suarez [8] test is shown in Figure 1. A snapshot of the global "weather patterns" at one year into the simulation can be seen in Figure 1c. Additional diagnostics were performed to compare to results and figures from the Held and Suarez [8] paper. The thermal structure, zonal-mean temperature, zonal-mean wind, and derived eddy statistics of the simulation (not shown here) all compare very well with the results shown in Figures 1c, 2, 3, 4, etc. of [8].

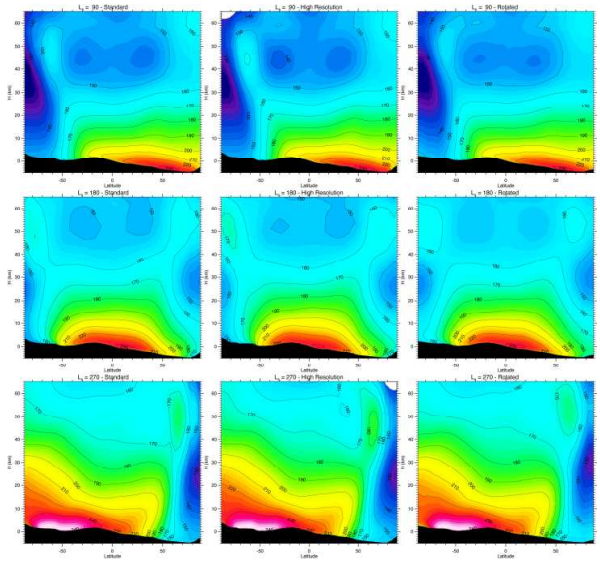

Figure 2: Zonal-mean temperatures (background color and contour lines) from a series of global MarsWRF simulations. The top row shows results at L_s=90°, while the middle row shows L_s=180°, and the bottom row L_s=270°. The left column shows results from the standard MarsWRF global setup (see text). The middle column shows results from a simulation run at twice the horizontal resolution. The right column shows results from a global simulation using the transverse cylindrical map projection.

Global Martian Validation Tests: Here we hope to confirm that the general circulation generated by the model agrees with other models and with observations to within the spread of uncertainty in current GCM simulations. The zonal-mean temperature structure and the zonal-mean zonal wind as simulated by the MarsWRF GCM standard simulation are shown for the two solstices and for northern autumnal equinox in Figure 2.

The cross sections of temperature are directly comparable to retrievals from TES data for the first MGS mapping year [9], using an averaging interval of 5° of L_s. The top model

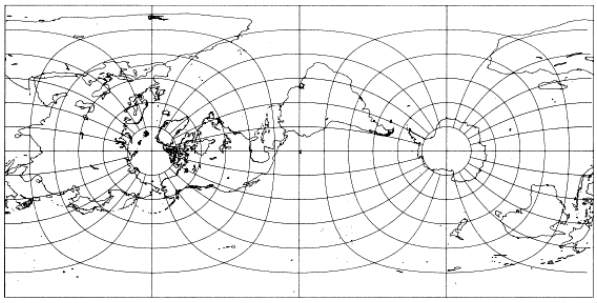

Figure 3: Transverse cylindrical ("rotated pole") map projection. This particular transverse transformation, with the north pole in the left center and the south pole in the right center and $\pm 90^{\circ}$ longitude running horizontally through the center, is called the "Cassini" projection.

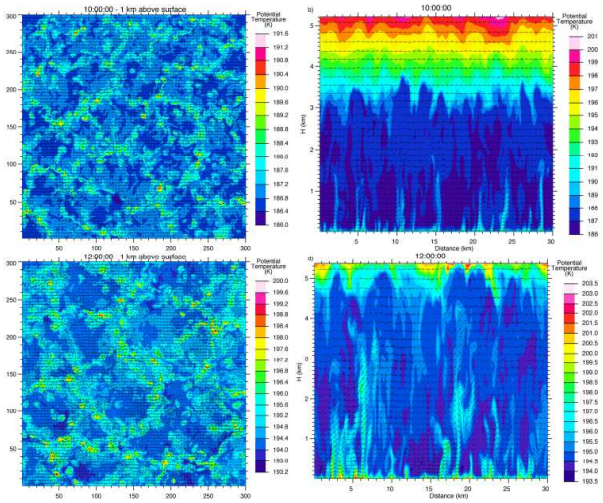

Figure 4: The growth of convective cells over 3 hours in a 300 x 300 large eddy simulation (LES) for Mars conditions. The plots on the left show potential temperature at a height of approximately 1 km, while those on the right show a vertical slice through the center of the domain (the model domain actually extends up to 10km in height, but only the lower half is shown here). The upper row is at 10 AM local time, and the bottom row at local noon. Note that the contour intervals vary from plot to plot.

layer is at a height of approximately 100 km. Each of the figures shows three columns and three rows. The rows represent northern summer solstice, southern spring equinox, and southern summer solstice. The three columns show the result of the model in three different configurations, the first one being a standard 64 x 36 x 25 (X x Y x Z) simulation, the second being a higher resolution at 128 x 72 x 25, and the third column being the same resolution as the first, but with a map projection using a rotated pole (described below). In all cases, the panels shown are from at least several years into a simulation.

The rotated pole (actually, the transverse cylindrical) projection is shown for a familiar planet in Figure 3. This map projection has the advantage of providing good and uniform resolution at the geographical poles, which should be of great use for simulation of the crucial Martian polar regions. Figure 2 shows that the zonal mean atmosphere simulated using the transverse cylindrical orientation is not significantly different from that generated with a traditional GCM computational grid.

Large Eddy Simulation (LES): A large eddy simulation uses a numerical model with sufficient resolution to explicitly simulate the larger eddies involved in boundary layer convection. WRF is amenable to LES application since it uses fully compressible, non-hydrostatic governing equations of motion. While the LES MarsWRF is designed to capture a large fraction of the turbulent eddy spectrum, computational reality still dictates a resolution too poor to capture the viscous or inertial subranges (i.e., LES MarsWRF uses grid spacings of at least a few meters). Here, we merely present some illustrative results from an initial LES simulation in Figure 4.

This simulation has a domain extent of 300 grid points in both horizontal directions and 100 in the vertical. With 100 m horizontal grid spacing, the domain thus covers 30 km by 30 km. In the vertical, an increasingly stretched grid covers 10 km, with the lowest layer about 20 m in thickness and with layer thicknesses increasing with height. The domain is double periodic, with no horizontal variations in topography or thermal properties. A uniform background wind of 7 m/s is applied to the entire horizontal domain at all heights.

The left column of Figure 4 shows variations in potential temperature that highlight the presence of convection cells defined by relatively thin, warm, upwelling sheets (the walls of approximately hexagonal convective cells), and much more expansive, cooler downwelling. This pattern is that of open cellular convection. The right column of Figure 4 shows vertical slices through the model at the middle of the domain. Near the surface, multiple plumes develop associated with the unstable environment, of which only some penetrate to great vertical extent. The reduction in the number of plumes penetrating to greater heights is directly associated with the filtering of small-scale cells with height in the horizontal plots. At the lowest levels, cells of various sizes are generated and these cells develop aspect ratios of between roughly 1 and 5, consistent with terrestrial boundary layer convection. Cells of small horizontal scales thus have correspondingly small vertical scales, and simply do not constitute part of the spectral population of cells at greater height.

Mesoscale Simulations: An example mesoscale application is shown here with an idealized simulation of flow in Valles Marineris and illustrated in Figure 5. The simulation is idealized in the sense that the domain is set to be doubly periodic, the local time is defined to be identical at all grid points on any given time step, and the Coriolis parameter is set to a uniform value across the domain. Our goal with the simulation was to examine slope flow on the canyon walls in

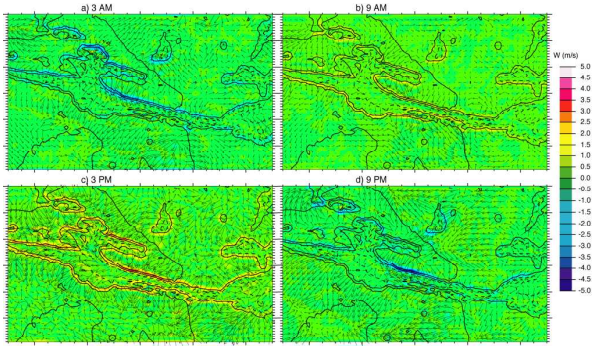

Figure 5: The diurnal cycle of winds in the Valles Marineris region on Mars, simulated by MarsWRF run as a mesoscale model with periodic horizontal boundary conditions. The background color shows vertical wind, and the arrows show horizontal wind (though only one in four wind vectors are shown for clarity). Local times shown are (a) 3AM, (b) 9AM, (c) 3PM and (d) 9PM. Unlabeled topography contours are shown for geographical reference.

the absence of local time variations and the influence of larger-scale flows. There is no large-scale background wind applied. The domain comprises 60 by 120 grid points in the horizontal (24 km spacing), with 25 vertical levels extending up to 40 km.

Valles Marineris provides one of the most significant regions of topographic relief on Mars. Figure 5 shows four local time snapshots of wind at approximately 80 m altitude. The simulation confirms the generation of upslope and downslope winds on the canyon walls of up to several m/s during the times of peak daytime heating and after sunset, respectively. These winds are particularly strong in the sector north of Coprates Chasma (to the east of the maximum north-south width of the canyon system). Flow inside the canyon is driven along the canyon axis, with generally downslope (east-to-west) flow at night and upslope flow during the daytime.

Current and Ongoing Research:

1. Dust cycle and storms. Simulations using interactive dust (radiatively and dynamically) are being undertaken, using lifting parameterizations that simulate small-scale convective processes (e.g., dust devils) and large scale wind stress. This work is focused on addressing control of the seasonal cycle of opacity, the dynamics of dust storm initiation and evolution, and the evolution of surface dust distributions.

2. Global water cycle. The global water cycle has been introduced into the MarsWRF model in the form of water vapor and water ice transport, exchange with evolving surface water ice caps, and recently, through the inclusion of a subsurface water diffusion and exchange model. Decadal length simulations focused on the control of the global water cycle and relationship with the dust cycle, are the goal of this study.

3. CO_2ice microphysics, and non-condensibles and the CO_2cycle. A detailed CO_2ice microphysics scheme has been implemented in MarsWRF, with the goal of both examining spacecraft observations inferred to represent CO_2ice clouds, and also with a view to paleoclimate, where CO_2clouds could have played an important role in climate. As a part of our broader study of the CO_2cycle, we have also included the ability for non-condensible gases (such as Ar) to accumulate when CO_2condenses (and *vice versa*). This allows for direct comparison with GRS data.

4. Orbital-variation climate change and ancient climates. Two main types of paleoclimate studies have been undertaken with the model so far. The first involves using essentially current values for volatile abundances, but examining how the climate shifts and evolves these volatiles when the orbital elements, and hence solar forcing patterns, change. The second involves increasing the amount of $CO_2$and adding additional greenhouse gases such as SO_2, to examine how the circulation and climate might have differed in the distant past.

References: [1] Richardson, M. I. and Wilson, R. J. (2002), *J. Geophys. Res.*, *107* (E5), Art. No. 5031. [2] Toigo, A. and Richardson, M. I. (2002), *J. Geophys. Res.*, *107* (E7), Art. No. 5049. [3] Skamarock, W. C. et al. (2005), *NCAR Technical Notes 468+STR*. [4] Michalakes, J. et al. (2004) *Proceedings of the 11th ECMWF Workshop on the Use of High Performance Computing In Meteorology*. [5] Arakawa, A., and Lamb, V. R. (1977), *Methods of Computational Physics*, *17*, 173–265. [6] Laprise, R. (1992), *Mon. Weath. Rev.*, *120* (1), 197–208. [7] Suarez, M. J. and Takacs, L. L. (1995), NASA Center for Aerospace Information (CASI), NASA-TM-104606-VOL-5, REPT-95B00069-VOL-5, NAS 1.15:104606-VOL-5, 19950401. [8] Held, I. M. and Suarez, M. J. (1994), *Bull. Amer. Met. Soc.*, *72* (10), 1825–1830. [9] Smith, M. D. et al. (2001), *J. Geophys. Res.*, *106* (E10), 23929–23945.